INTERFACE

royalsocietypublishing.org/journal/rsif

Research

Cite this article: Chhajer H, Rizvi VA, Roy R. 2021 Life cycle process dependencies of positive-sense RNA viruses suggest strategies for inhibiting productive cellular infection. *J. R. Soc. Interface* **18**: 20210401. https://doi.org/10.1098/rsif.2021.0401

Received: 14 May 2021
Accepted: 18 October 2021

Subject Category:
Life Sciences–Mathematics interface

Subject Areas:
systems biology

Keywords:
positive sense RNA virus, viral intracellular life cycle model, compartment formation dynamics, stochastic fate of infection, synergy in virus inhibition

Author for correspondence:
Rahul Roy
e-mail: rahulroy@iisc.ac.in

Electronic supplementary material is available online at https://doi.org/10.6084/m9.figshare.c.5680531.

THE ROYAL SOCIETY PUBLISHING

Life cycle process dependencies of positive-sense RNA viruses suggest strategies for inhibiting productive cellular infection

Harsh Chhajer[1], Vaseef A. Rizvi[2] and Rahul Roy[1,3]

[1]Centre for Biosystems Science and Engineering, [2]Molecular Biophysics Unit, and [3]Department of Chemical Engineering, Indian Institute of Science, Bangalore 560012, Karnataka, India

HC, 0000-0001-9252-1855; RR, 0000-0003-3329-8803

Life cycle processes of positive-strand (+)RNA viruses are broadly conserved across families, yet they employ different strategies to grow in the cell. Using a generalized dynamical model for intracellular (+)RNA virus growth, we decipher these life cycle determinants and their dependencies for several viruses and parse the effects of viral mutations, drugs and host cell permissivity. We show that poliovirus employs rapid replication and virus assembly, whereas the Japanese encephalitis virus leverages its higher rate of translation and efficient cellular reorganization compared to the hepatitis C virus. Stochastic simulations demonstrate infection extinction if all seeding (inoculating) viral RNA degrade before establishing robust replication critical for infection. The probability of this productive cellular infection, 'cellular infectivity', is affected by virus–host processes and defined by early life cycle events and viral seeding. An increase in cytoplasmic RNA degradation and delay in vesicular compartment formation reduces infectivity, more so when combined. Synergy among these parameters in limiting (+)RNA virus infection as predicted by our model suggests new avenues for inhibiting infections by targeting the early life cycle bottlenecks.

1. Introduction

Positive sense single stranded RNA ((+)RNA) viruses, that include *Enteroviridae* (poliovirus), *Flaviviridae* (Dengue virus), *Coronaviridae* (SARS coronavirus) virus families, are a major public health challenge. Better understanding of the cellular viral dynamics can help us identify new drug targets and novel antiviral approaches. The virus grows inside the cell using a complex set of molecular and cellular processes that has evolved to ensure successful propagation. (+)RNA viruses sequentially translate viral proteins using their positive strand RNA genome upon cell entry, replicate to form nascent genomes from a double stranded RNA (dsRNA) replication intermediate and create new virus particles by encapsidating the newly synthesized (+)RNA genomes with structural proteins. Members of this class show significant diversity in genome size, physical makeup, constituent viral proteins, host tropism and chronicity of infection. Yet, they also display striking similarities in cellular life cycle processes and their dynamics, closely imitating mechanisms of replication, translation, virus assembly as well as analogous interactions with the host cell machinery. This has motivated the search for universal features that can be exploited as broad spectrum anti-viral targets.

One common characteristic of most (+)RNA viruses is the induction of significant alterations of the intracellular host membranes [1–4]. The vesicular membranous structures formed provide a conducive micro-environment for efficient viral replication, protect the viral RNA and proteins from cytosolic degradation and host defence systems, and hence are also referred to as vesicular compartments (CMs). Impeding membrane reorganization has been shown to decelerate cellular infection dynamics [5,6], lower viral yield [7–10] and reduce

the propensity of the virus to establish cellular infection in the host cell [6,11,12]. In general, failure to establish viral infection has been associated with cellular heterogeneity and is attributed to the random loss of genome segments by RNA degradation in the early stages of infection [13–15]. This stochastic effect manifests at low multiplicity of infection [12] and is observed across several virus families. While this suggests that early events in the virus life cycle determine the fate of infection, what factors control this mode of viral clearance have not been examined in detail.

Quantitative measurements and mathematical modelling have tremendously enhanced our understanding of how the subtleties of intracellular processes shape the outcome of viral infections [16–26]. Understanding derived from these and combined with their extensions that incorporate extracellular and immune response have been used to determine effectiveness of interventions and combinations thereof [27–31]. However, detailed models with explicit molecular details suffer from redundancy in fitting parameters or challenges with estimating parameters experimentally. On the other hand, simplistic generalized models can fail to accurately emulate the experimentally observed dynamics across a large class of viruses, viral mutations and different host cells. Nevertheless, viral dynamics models can be insightful if they universally capture experimental observations while allowing sufficient inference of molecular mechanisms across viruses. Apart from identifying life cycle bottlenecks, they can be employed to predict the effectiveness of broadly applicable anti-viral strategies.

Most prior intracellular +RNA viral dynamics models also do not account for the slow formation kinetics of the membranous vesicular compartments. Since this event coincides with a period sensitive to stochastic fluctuations in viral RNA, it is unclear how membrane reorganization influences the virus life cycle. In this study, we extend previous viral dynamics models [17,19,22] by incorporating the kinetics of vesicular compartment formation post infection. We show that our model now accurately captures several variants of experimentally measured dynamics for hepatitis C virus (HCV) [22], Japanese encephalitis virus (JEV) [32] and poliovirus (PV) [19] infection from the literature. Indeed, incorporation of vesicular compartment formation dynamics is able to explain the discrepancy in PV viral dynamics observed with earlier models. Our model further identifies differences among virus life cycle properties and dynamics including observed effect of viral mutations [5] and host factor silencing [5,7] without modifications. Our results also reveal that the dynamics of compartment formation is a critical kinetic bottleneck for the viruses. Using our estimate of life cycle parameters, we quantify the ability of the viruses to establish a productive infection upon entry into the host cell that we refer to here as 'cellular infectivity' (Φ). Apart from the formation of CM, we recognize limiting replication, increased cytoplasmic degradation of viral RNA and reduction in translation as pan-viral inhibition strategies. Furthermore, we estimate the synergy among these strategies that can limit cellular infectivity providing opportunity to clear the viral infection.

2. Results

2.1. Cellular viral life cycle model for monopartite (+)RNA viruses

We propose a mathematical model for cellular life cycle of single stranded monopartite (+)RNA viruses (figure 1*a*; details in electronic supplementary material, S1). We focus on intracellular processes common to such viruses and it is inspired by previous HCV and PV models [17,19,22] (equations (2.2)–(2.7), table 1). Upon entry into the cell, viral (+)RNA in cytoplasm (R_{cyt}) is translated (by host ribosomes) to produce structural (P_S) and non-structural (P_{NS}) proteins at a rate k_t (equations (2.3) and (2.4)).

Though translation occurs in the cytoplasm, replication is mainly restricted to vesicular compartments (CMs) [1,2]. CM formation occurs via extensive alteration to host intracellular membranes [33,34] induced by viral and host proteins post infection [1–3,35]. Although a slow and critical step conserved across many (+)RNA viral life cycle, previous models did not account for their gradual formation. We hypothesized that this delay in formation of vesicular compartments will result in major limitation to viral growth either due to early degradation of viral RNA or late onset of replication dominant phase. Therefore, we incorporate the CM formation dynamics explicitly in our model using a functional form based on analysis of cellular ultrastructure characterization (figure 1*b*; electronic supplementary material, figure S1). Assuming that host membrane homeostasis limits the extent of alterations, we use the popular Weibull function [36] to model the normalized growth of vesicular compartments, f_{CM} (equation (2.1)):

$$f_{CM} = 1 - e^{-(t/\tau_S)^n}. \tag{2.1}$$

τ_S parameterizes the time scale of the structural manifestation of CMs whereas n defines the steepness of the function. Figure 1*b* shows that increase in vesicular membranous structures observed for (+)RNA viruses is indeed virus and strain specific [37–40]. Though the value of τ_S does not vary significantly, fitting improves as n increases from 2 to 4, suggesting some level of synchrony in CM development (electronic supplementary material, table S1). Interestingly, τ_S estimates correlate with the time scale of cellular infection across viruses and strains (as observed for the Zika strains [41]) suggesting the central role of host membrane remodelling in defining viral growth dynamics. Our estimate for the τ_S for ZIKV (13.3 h for MR766 and 23.7 h for H/PF/2013 strain) is also consistent with the time interval (approx. 16 h post infection) beyond which addition of a membrane reorganization inhibitor (K22) is ineffective as an antiviral [9] further emphasizing the importance of CM formation in viral dynamics.

In context of viral replication, one must consider the ability of these sites to provide protective confinement for the RNA replication complex but this aspect has not been quantitatively characterized to date. We argue that the structural and functional aspects of CM formation are likely to be correlated. Therefore, we use the same functional form (equation (2.1) with $n = 4$), but consider a different time parameter (τ_F) to model the functional maturation of CMs for replication hereon. Although not explicitly incorporated, τ_F also subsumes other delays associated with virus entry and genome uncoating (see electronic supplementary material, S2). However, such delays have been shown to be comparatively smaller supporting our assertion that CM formation forms the major bottleneck to viral growth upon infection [19,22,42].

Cellular homeostasis (posed by host cell proteome and lipid homeostasis) limits the number of available CMs and

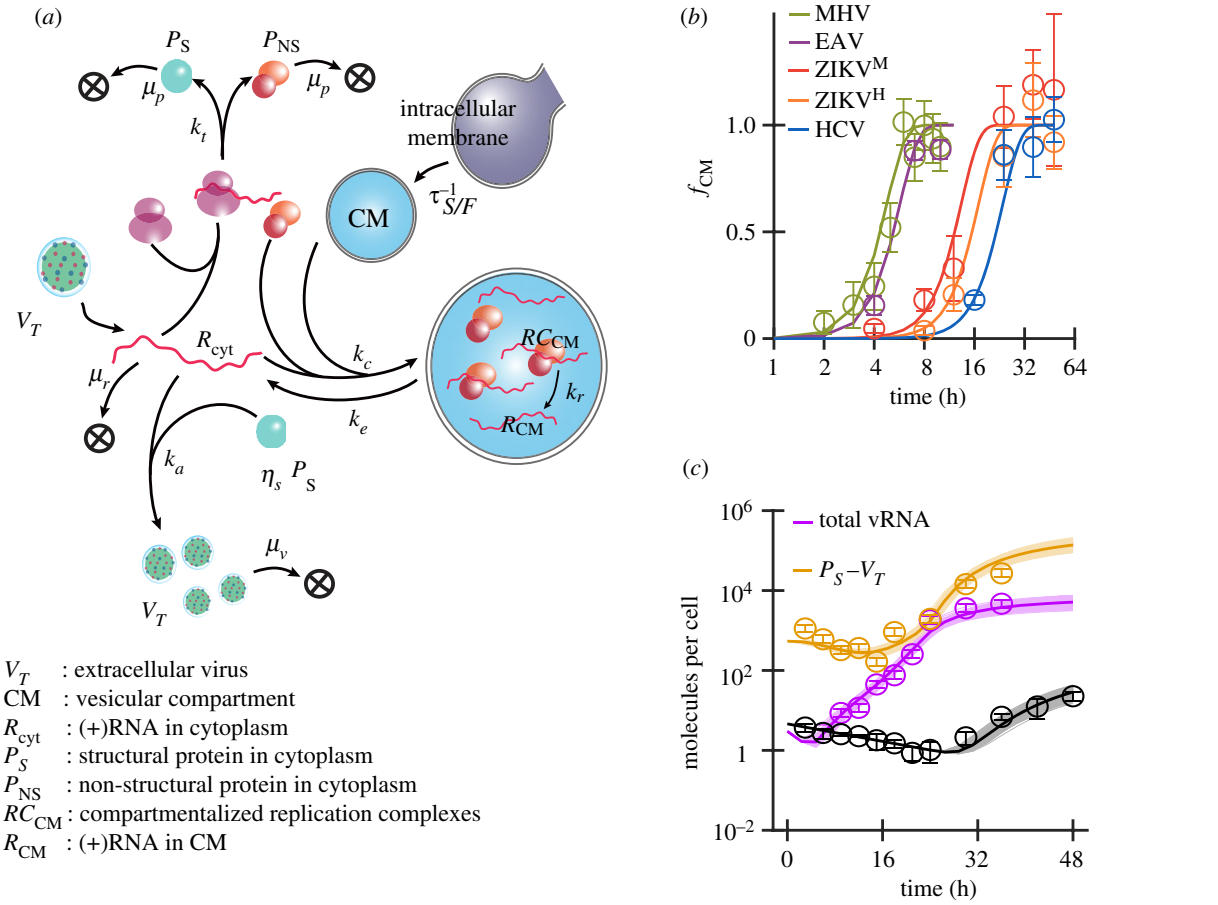

V_T : extracellular virus
CM : vesicular compartment
R_{cyt} : (+)RNA in cytoplasm
P_S : structural protein in cytoplasm
P_{NS} : non-structural protein in cytoplasm
RC_{CM} : compartmentalized replication complexes
R_{CM} : (+)RNA in CM

Figure 1. Viral life cycle model and compartment formation dynamics. (*a*) Schematic of the viral life cycle model. In the cytoplasm, the (+)RNA (R_{cyt}) is translated by the host ribosomes to produce viral structural (P_S) and non-structural proteins (P_{NS}). Intracellular membrane is reorganized to form compartments (CM) which harbour viral replication complex (RC_{CM}) that produce new (+)RNA strands, which are exported out into the cytoplasm. η_S copies of P_S associate with R_{cyt} to assemble virus particles (V_T). (*b*) Normalized dynamics of compartment formation (f_{CM}) observed for different (+)RNA viruses fitted (lines) using equation (2.1) ($n = 4$) is shown. Data are derived from [37–40] for mouse hepatitis virus (MHV), equine arteritis virus (EAV), MR766 and H/PF/2013 strains of Zika virus (ZIKV^M and ZIKV^H) and hepatitis C virus (HCV). (*c*) Virus life cycle model fit for HCV infection in Huh7 cells [22]. Circles and error bars correspond to data and coloured lines represent respective fits. Thin lines (lightly coloured in background) represent the dynamics predicted using a set of best parameter combinations (250 sets) from iABC and thick lines denotes their corresponding average.

hence replication complexes (formed by R_{cyt} and P_{NS}) compete for the unoccupied compartments given by [$f_{CM} - (RC_{CM}/N_C)$], where RC_{CM} denotes the number of compartmentalized replication complexes and N_C is the carrying capacity for RC_{CM} (table 1). Therefore, we model the compartmentalization of replication with a logistic function (equations (2.2), (2.4), (2.5)). RC_{CM} synthesize new (+)RNA strands at a rate, k_r (equation (2.6)). The (+)RNA in the compartments (R_{CM}) are exported out into the cytoplasm at rate, k_e (equations (2.2) and (2.6)), where it can re-participate in the cycle. While the viral RNA and proteins degrade in the cytoplasm, we ignore degradation in the compartments [2,4,26]. Finally, viral assembly occurs in cytoplasm where a R_{cyt} associates with η_S molecules of P_S to produce extracellular viral particles (V_T) at an overall rate of k_a (equations (2.2), (2.4), (2.7)).

Cellular life cycle model

$$\frac{dR_{cyt}}{dt} = k_e \,.\, R_{CM} - k_a \,.\, P_S \,.\, R_{cyt} - \mu_R \,.\, R_{cyt} - k_c \,.\, P_{NS} \,.\, R_{cyt} \left(f_{CM} - \frac{RC_{CM}}{N_C}\right) \tag{2.2}$$

$$\frac{dP_{NS}}{dt} = k_t \,.\, R_{cyt} - \mu_P \,.\, P_{NS} - k_c \,.\, P_{NS} \,.\, R_{cyt} \,.\, \left(f_{CM} - \frac{RC_{CM}}{N_C}\right) \tag{2.3}$$

$$\frac{dP_S}{dt} = k_t \,.\, R_{cyt} - \eta_S \,.\, k_a \,.\, P_S \,.\, R_{cyt} - \mu_P \,.\, P_S \tag{2.4}$$

$$\frac{dRC_{CM}}{dt} = k_c \,.\, P_{NS} \,.\, R_{cyt} \,.\, \left(f_{CM} - \frac{RC_{CM}}{N_C}\right) \tag{2.5}$$

$$\frac{dR_{CM}}{dt} = k_r \,.\, RC_{CM} - k_e \,.\, R_{CM} \tag{2.6}$$

and

$$\frac{dV_T}{dt} = k_a \,.\, P_S \,.\, R_{cyt} - \mu_V \,.\, V_T. \tag{2.7}$$

2.2. Model recapitulates observed hepatitis C virus life cycle dynamics

Using an iterative approximate Bayesian approach (iABC; see Methods and electronic supplementary material, SM1), we fit our life cycle model to the dynamics of intracellular viral RNA, proteins, and extracellular viruses observed previously. In the iABC algorithm, we sample the current distribution of estimates in the multi-dimensional parameter space efficiently using Latin hyper-cube sampling [43]. We select a subset of the sampled parameter combinations, whose predictions have lowest deviation from the experimental data, to update the distribution. We report the distribution instead of point estimates for the parameters and introduce uniform

Table 1. Life cycle model parameters.

parameter (units)	description	HCV in Huh7	JEV in PS	PV in HeLaS3
free parameters[a]				
τ_F (h)	time constant for functional development of CMs	5.8	2.6	4.2
k_t (h^{-1})	protein production rate per R_{cyt}	23.7	1.6×10^{2}	18.9
k_c (molecules^{-1} h^{-1})	formation rate of RC_{CM}	2.6×10^{-3}	1.6×10^{-2}	1.2×10^{-2}
k_r (h^{-1})	(+)RNA synthesis rate per RC_{CM}	3.6	3.7	2.2×10^{2}
k_e (h^{-1})	export rate of R_{CM} into the cytoplasm	6.6×10^{-2}	7.2×10^{-2}	1.1
N_C (number)	RC_{CM} carrying capacity of the host cell	8.8×10^{1}	1.21×10^{3}	1.62×10^{3}
k_a (molecules^{-1} h^{-1})	effective virus generation rate	3.6×10^{-8}	8×10^{-9}	5.6×10^{-3}
fixed parameters[b]				
η_S	number of P_S per virus particle	180	180	60
μ_R (h^{-1})	degradation rate of R_{cyt}	0.25	0.25	0.25
μ_P (h^{-1})	degradation rate of P_S and P_{NS}	0.11	0.11	0.11
μ_V (h^{-1})	degradation rate of V_T	6×10^{-3}	6×10^{-3}	6×10^{-3}

[a]Median of the distribution estimated from data fitting (figure 2*c*).
[b]From literature [22,56–58] or from analysis of [22], as shown in electronic supplementary material, S9.

noise to the distribution in each iteration (electronic supplementary material, SM1) making it less sensitive to sampling biases and local minima. Starting with a uniform prior distribution of parameter values, we first recover model parameter estimates using this approach for the well-characterized HCV infection in Huh7 cells [22] (figure 1*c* and table 1; electronic supplementary material, table S2). We find that new (+)RNA strands are produced at (k_r =) 3.6 h^{-1} per compartmentalized replication complex (RC_{CM}). Using RNA polymerization rate of 150 nt min^{-1} [44], we predict that on average ≈4 simultaneous replication events occur per RC_{CM}. This is consistent with experimental observations of synthesis of multiple viral RNA per replication intermediate (reported to be 5 for the closely related Dengue virus [45]). Similarly, our prediction for the steady-state ratio of viral (+)RNA to (−)RNA (=54 : 1) compares well with the experimentally observed ratio of 30 : 1 [46,47].

While differences in parameter definitions limit exact comparison, we find good agreement with previous efforts to model HCV dynamics. For example, assuming that 10 ribosomes [48] translate the viral RNA at a time and $k_t = 23.7$ h^{-1}, we predict the HCV protein production rate to be 2.4 h^{-1} per RNA. This is comparable to the previous estimate of the rate-limiting step in protein synthesis (polyprotein cleavage rate, 1 h^{-1} [16,17]). Our prediction for (+)RNA export out of vesicular compartments is also similar to previous estimates [16]. However, virus production in our model is 50-fold faster than previous estimates. We attribute this to the unaccounted delay in CM formation in prior models that contributes to reduction in their effective assembly rates [22]. Therefore, we were able to recapitulate HCV experimental observations that were not built *a priori* into the model as well as match previous estimates for comparable parameters.

To further validate our model, we evaluate the life cycle dynamics of subgenomic HCV (sgHCV) transfected into Huh7 (Huh7-Lp) cells and its more permissive derivative (Huh7-Lunet) cells [17] (electronic supplementary material, figure S2). Our estimates for k_t, k_r and k_c (the rate of formation of RC_{CM}) for the subgenomic viral transfection are similar to corresponding estimates for full-genomic HCV infection (electronic supplementary material, tables S2 and S3) suggesting the robustness of our model across different experimental systems for HCV. However, the sgHCV system exhibits delayed RC formation and faster (+)RNA export out of CM compared to the virus infection. This may be likely due to lack of structural proteins, transfection induced cellular artefacts or additional pre-processing of transfected RNA [17]. When we compare the sgHCV dynamics in the two cell lines, the highly permissive Huh7-Lunet cells exhibit faster CM formation (1.9 fold lower τ_F) and higher stability of viral dsRNA replication intermediate (11.8 fold larger N_C) compared to Huh7-Lp cells [49], suggesting efficient replication compartmentalization is correlated with higher cellular permissivity of HCV infection (electronic supplementary material, table S3). This again emphasizes that CM formation dynamics should be considered a critical aspect of (+)RNA viral dynamics models.

2.3. Comparative analysis of monopartite (+)RNA viruses

To understand the differences in life cycle properties among (+)RNA viruses, it is pertinent to compare same model parameters across viruses. Attempts at such comparisons have been challenging due to vast differences among the dynamics of different viruses. Since our model explicitly accounts for observed kinetics of vesicular compartment formation that can be dramatically different among viruses, we asked if our model can capture viral growth dynamics of two additional families of viruses for which comprehensive viral dynamics data exist, namely *Enteroviridae* (PV [19]) and *Flaviviridae* (JEV [32]). Our model fits the dynamics of viral RNA, proteins and extracellular virus well for both these viruses from two independent studies (figure 2*a*,*b*). Comparison of life cycle process parameters (estimated distributions shown in figure 2*c*, and summarized in table 1 and electronic supplementary material, table S2) shows that the replication rate (k_r) and export rate of (+)RNA from compartment (k_e)

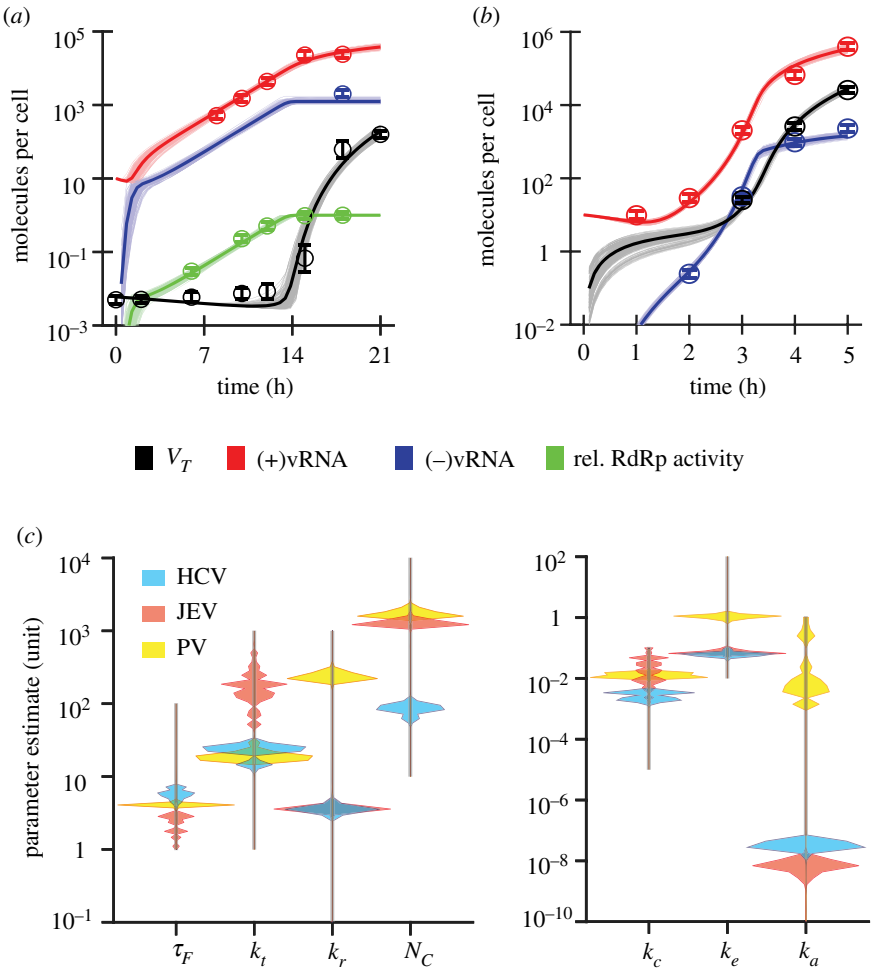

Figure 2. Comparison of monopartite (+)RNA viruses. Model fits (thin lines, average shown as a thick line) for the intracellular dynamics of virus constituents in case of (*a*) JEV infection in PS cells [32] and (*b*) PV infection in HeLaS3 cells [19] are shown. (*c*) Comparison of parameter value distributions estimated for HCV, JEV and PV life cycle dynamics from model fitting. Grey vertical lines indicate the range of initial guesses used for each parameter.

exhibit virus family specific trends (figure 2*c*). For example, PV RNA replicates rapidly (60-fold higher k_r) and re-enters the cytoplasmic pool faster (16-fold higher k_e) than *Flaviviridae* family (HCV and JEV). Using our estimate of $k_r = 210\ \mathrm{h}^{-1}$ for PV (similar to $133\ \mathrm{h}^{-1}$ estimated earlier [19]) and assuming PV genome replication takes 100 s [50], we predict 5.8 simultaneous replication events occur per RC_{CM} closely matching previously measured values of 6.5–7 [51,52]. On the other hand, JEV displays ≈3.8 simultaneous replications per RC_{CM} (assuming RNA elongation rate of $150\ \mathrm{nt\ min}^{-1}$ [44]) comparable to HCV and Dengue as discussed above. This further shows that our model captures the now well recognized fact that CMs are sites of multiple parallel replication reactions without explicitly assuming it [2].

Protein synthesis rate $k_t = 18.9\ \mathrm{h}^{-1}$ for PV is comparable to HCV and similar to a previous report [19] but JEV protein synthesis is seven times faster. Although polyprotein processing and host cell features affect k_t, we attribute the high k_t values for JEV to its RNA cap-dependent translation initiation [53] compared to the IRES mediated mechanism employed by HCV and PV [54,55]. Faster protein production and an associated early induction of membrane reorganization could also contribute to the faster functional maturation of CM for JEV consistent with our estimates for τ_F.

Virus assembly and generation defined by k_a is significantly (greater than 10^5 fold) faster for PV compared to the *Flaviviridae* viruses (HCV and JEV) reflecting their corresponding complexity in assembly and maturation. While the detailed mechanisms of virus assembly remain poorly understood, HCV and JEV are enveloped viruses made of 180 copies of three different structural proteins [56,57] that require maturation post assembly whereas PV is a smaller non-enveloped virus [58].

Since it is a common concern in multi-parameter fitting, we tested whether the parameter estimates for each virus were sensitive to the initial guesses or the choice of the prior distribution. Compared to figure 2*c* that depicts the estimated parameter distributions when a uniform prior distribution is employed, we also estimated the posterior distributions for JEV and PV life cycle parameters but using a HCV posterior distribution (as obtained in figure 2*c*) as the prior distribution. Despite employing a highly skewed prior distribution, we find that the parameter estimates for both JEV and PV are largely unaffected (electronic supplementary material, figure S6). This confirms that the observed differences in parameter estimates are specific to the corresponding viral life cycle dynamics.

The differences in virus life cycle parameters are also robust to alternative model formulations (electronic supplementary material, S5). For example, whether we consider a more gradual rise in compartments (Weibull exponent, $n = 2$) for vesicular compartment formation (electronic supplementary material, figure S7) or pre-formed CM ($f_{\mathrm{CM}} = 1$) (electronic supplementary material, figure S8), high rates for JEV translation,

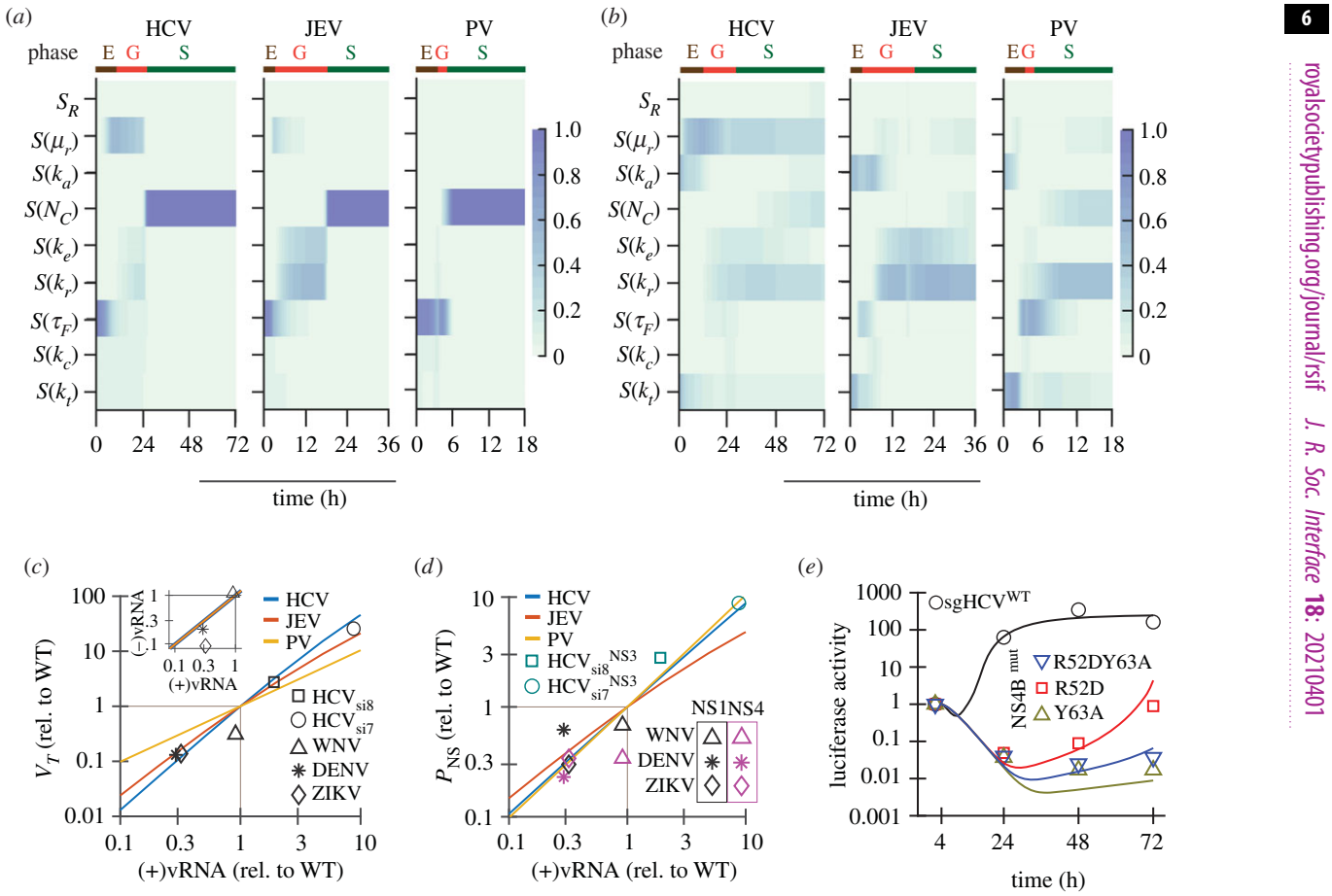

Figure 3. Perturbation analysis of viral life cycle parameters. Parameter-temporal sensitivity profiles for dynamics of (*a*) RC_{CM} and (*b*) V_T, for HCV, JEV and PV (with initial seeding of $R_{cyt} = 3$) are shown. $S(X)$ denotes the profile associated with parameter, X, and $S_R = S(\mu_P) + S(\mu_V) + S(dummy)$. Based on the RC_{CM} profiles, life cycle of each of the viruses can be divided into the establishment (E), the growth (G) and the saturation (S) phases as shown. Time axis is not to scale across profiles for different viruses. Fold change in steady state levels (*c*) V_T versus (+)RNA, (*d*) P_S versus (+)RNA and (*c*, inset) (−)RNA versus (+)RNA, due to change in N_C is compared to experimental data [7,5]. Solid lines are model predictions and symbols show experimental data. (*e*) Viral protein dynamics for NS4B mutants is fitted with the life cycle model by varying τ_F. Solid lines and symbols show best fits and data [5], respectively.

and rapid replication and assembly of PV set them apart (electronic supplementary material, table S4). Similarly, stoichiometry of P_{NS} in formation of RC_{CM} (electronic supplementary material, figure S9), or consideration of replication coupled assembly of viral particles [22] (electronic supplementary material, figure S10) does not alter our virus-specific parameter estimates. While goodness of fit based on cumulative AIC values for the three viruses (electronic supplementary material, table S4) demonstrates only a marginal advantage in favour of our main model, measured CM formation dynamics [33,34] support our choice of the model. Corroboration with independent experimental data like recovery of steady-state levels of replication intermediate [17,59,60] and steady-state positive/negative RNA ratios [46,47] (electronic supplementary material, table S4) further supports our model. Due to the lack of molecular details for virus assembly, our model only qualitatively captures the virus assembly and release dynamics and we cannot discriminate between alternative sites (CMs versus cytoplasm) for virus assembly.

2.4. Conserved and virus-specific determinants shaping viral life cycle

With the ability to describe viral dynamics across a broad range of (+)RNA viruses, we evaluated how perturbations in life cycle model parameters affect the viral dynamics using temporal sensitivity analysis (TSA) with the eFAST algorithm [61]. TSA profiles for RC_{CM}, the key intermediate and a surrogate for viral replication, highlight three distinct phases for the viruses (figure 3*a*). The initial establishment (E) phase is sensitive to the delay in formation of CM (τ_F), and displays minimal replication due to shortage of CM. The next growth (G) phase represents the rapid increase in viral RNA production and is influenced by parameters governing the increase of (+)RNA in the cytoplasm, and thus the formation of dsRNA replication intermediate. Growth phase is sensitive to changes in viral replication rate (k_r), the kinetics of (+)RNA export from CM (k_e) and the rate of cytosolic degradation of (+)RNA (μ_R). The final saturation (S) phase is defined by the pseudo-steady state behaviour primarily regulated by the carrying capacity for RC_{CM} (N_C). Though the TSA trends are qualitatively similar, the time associated with each phase varies with the virus. The length of the E phase correlates with the estimate for τ_F, and time span of growth phase reflects k_r^{-1} and k_e^{-1}. Therefore, while the G phase is comparable for HCV and JEV, it is very short for PV as is evident with the rapid increase in PV RNA in a short window of 2 h [19].

Differences in the TSA profiles across the viruses are more evident when V_T (figure 3*b*) and R_{cyt} (electronic supplementary material, figure S11) are considered. The profiles associated with V_T are particularly informative in identifying

'choke points' and their effectiveness for different viruses. We postulate that perturbations to replication (k_r) would be more effective than translation (k_t) against JEV but vice versa for inhibiting PV growth. For HCV, viral dynamics is influenced by viral RNA degradation (μ_R) to a large extent followed by translation and replication. μ_R is critical for HCV life cycle as its (+)RNA has a large dwell time in the cytoplasm (due to its large τ_F, k_t^{-1} and k_c^{-1}). Thus, the model parameter sensitivity can generate virus-specific insights into life cycle intervention strategies that can be examined in the future.

2.5. Changes in N_C and τ_F mimic the effect of perturbations to compartment formation

Among the critical parameters discussed above, τ_F, k_e and N_C are reflective of the CM formation dynamics and its architecture. Various viral [1,2,4,7,35,62] and host perturbations [63–66] and drug interventions [8–10] have been reported to alter membrane reorganization, which ultimately affects infection kinetics as well as the steady state achieved in the later stages. To test how the dynamics of CM generation defines the virus life cycle, we emulate some of these perturbations by varying τ_F (for kinetics) and N_C (for steady state) and compare it to experimental observations.

Reticulon 3 (RTN3), an endoplasmic reticulum (ER) shaping host protein, is involved in ER membrane reorganization during various (+)RNA viral infections [63,64]. Silencing RTN3 in host cells reduces viral replication of flaviviruses [7] and enteroviruses [6], but increases it in the case of HCV [5]. In our model, N_C is the sole parameter that affects the steady state levels of viral (−)RNA levels (RC_{CM}), which is perturbed upon RTN3 silencing in host cells [7]. By just varying N_C, we are able to reproduce correlated fold changes in (−)RNA levels, viral titre and P_{NS} with respect to viral RNA as observed for various flaviviruses [7] and HCV [5] upon silencing RTN3 (figure 3*c*-inset, *c*,*d*). This also confirms that the model appropriately emulates the steady-state level correlations among the various virus constituents.

Our steady-state level relations for levels of virus and viral protein with viral (+)RNA are distinct for the three viruses considered here. For HCV and PV, P_{NS} varies linearly with viral (+)RNA level; however it is sub-linear in the case of JEV (figure 3*d*). The increase in V_T with viral (+)RNA levels is super-linear and sub-quadratic for JEV and HCV, respectively, whereas it is linear for PV (figure 3*d*). These trends are corroborated by steady-state analysis of the model (see electronic supplementary material, S3). Efficient assembly for PV ($k_a R_{cyt} >> \mu_P$) leads to R_{cyt}-independent level of P_S ($P_S \approx k_t/\eta_S k_a$), resulting in linear relation between V_T and (+)RNA ($V_T \approx k_r N_C/\mu_R \approx R_{cyt} k_t/\mu_R \eta_S$). The analysis also suggests that when comparing HCV and JEV, higher $k_t.k_a$ estimate contributes to faster assembly of R_{cyt}. Thus, R_{cyt} (and consequently $P_{NS} = k_t R_{cyt}/\mu_P$) increases sub-linearly with N_C for JEV.

To evaluate the effect of the compartment formation kinetics on the viral dynamics, we compare viral polyprotein dynamics of HCV NS4B mutants, shown to be defective in inducing membrane reorganization [35,62]. Using τ_F as the sole fitting parameter (details in electronic supplementary material, SM3), the model is able to accurately recapitulate the normalized protein dynamics observed for these sgHCV mutants [5] (figure 3*e*). The estimated τ_F for the NS4B sgHCV mutants R52D, Y63A and R52DY63A are 63, 101 and 80 h, respectively, compared to 5.8 h for the WT virus highlighting how increased delay in CM formation affects viral dynamics.

2.6. Compartmentalization of replication defines the fate of virus infection

Compartmentalization of viral replication establishes sites for efficient (+)RNA replication, protected from cytoplasmic degradation in the infected cell and leading to the rapid replication of the viral RNA. However, compartmentalization is not guaranteed upon virus entry, with the possibility of degradation of viral genome in the host cytoplasm before membrane reorganization. Previous models that assume pre-existing CMs do not envision this scenario. We posit that the infection outcome of viral seeding event is an all-or-none phenomenon that is determined at the onset of the infection by the opposing effects of cytoplasmic viral RNA degradation and the formation of RC_{CM} (figure 4*a*). Indeed, stochastic simulations of the HCV life cycle demonstrate these two outcomes akin to a previous report [26] (figure 4*b*). All realizations where RC_{CM} is formed before the complete degradation of viral RNA result in a productive infection, otherwise the infection extinguishes.

Predictions of PV (+)RNA dynamics during infection using a semi-stochastic simulation (see Methods) also support CM formation delay acting as a major bottleneck to viral dynamics (figure 4*c*). Compared to our main model (M_4^1), similar simulations with the pre-formed CM model (M', using its estimate; electronic supplementary material, table S4) do not match the observed dynamics (figure 4*c*). Such discrepancy is not explicitly evident when comparing the two models for HCV and JEV dynamics. Unlike PV, a very small lag is predicted by the main model as τ_F for HCV and JEV is a small fraction of their total cellular infection time-span. Furthermore, due to their small replication rates (k_r, compared to that of PV) the effect of the lag in CM formation is not amplified (discussed in electronic supplementary material, S5). Yet our main model is able to capture the dynamics for all viruses considered here where other models fail.

We define the likelihood of productive infection establishment (as observed in figure 4*b*) as the 'cellular infectivity', Φ. Φ ranges between zero (complete extinction of infection) and one (establishment of productive infection). We find that this infectivity is influenced by virus–host factors that are critical in the early stages of virus life cycle. For example, Φ increases monotonically until saturation to one with increasing viral seeding (N, the effective number of viral genomes present in the cell upon entry) (figure 4*d*). Similarly, it is modulated by the kinetics of viral processes contributing to the compartmentalization of replication (k_t, τ_F^{-1}, k_c) and the stability of viral genome in the host cytoplasm (μ_R^{-1}) (figure 4*d*,*f*; electronic supplementary material, figures S12 and S14). Similar reduction in infection success rate has been reported when CM formation is hindered by phosphatidylinositol 4-kinase III alpha silencing [11] or in the case of enterovirus mutations [6]. When compartment formation dynamics is not considered (M' model), cellular infectivity predicted is comparable for HCV and JEV but for PV it suggests that negligible infection can be achieved even with multiple infectious viruses per cell ($\Phi < 0.15$ at $N = 4$).

While universally predicted for many RNA viruses that employ some form of effective sequestering to achieve efficient replication, we can now estimate cellular infectivity

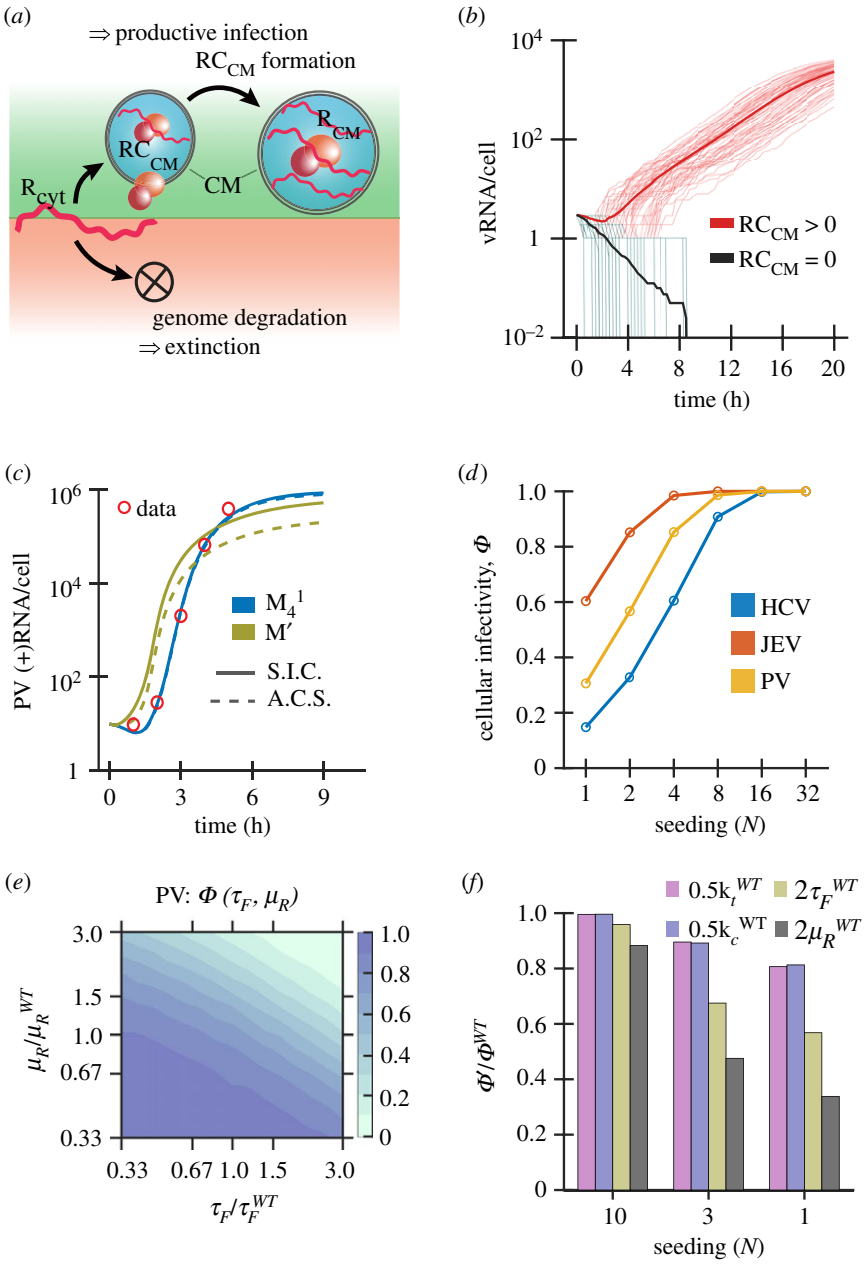

Figure 4. Stochastic fate of viral infection. (*a*) Schematic shows two disparate outcomes for viral genomes in the cell. When the cytoplasmic viral RNA is encapsulated in vesicular compartments, high replication rate and minimal degradation lead to productive infection. Otherwise, degradation of all viral RNA in the cytoplasm leads to complete extinction of the infection. (*b*) Stochastic realizations of cellular life cycle dynamics of HCV in Huh7 cells at viral seeding of 3. Thin lines show simulated trajectories for viral RNA (red) when at least 1 RC_{CM} was formed or (black) when no RC_{CM} were formed and thick lines represent their corresponding averages. (*c*) Average dynamics of PV (+)RNA molecules per cell predicted using the main model (M_4^1, blue lines) and the pre-formed CM model (M', olive green lines), compared with experimental observation [19] (open red circles). We consider a seeding of 10 PV RNA to initialize each semi-stochastic realization; averaging was done either over successfully infected cells (S.I.C., solid lines) or over all cells seeded (A.C.S., dashed lines). (*d*) Probability of establishment of infection (Φ) as a function of seeding number (N) for HCV, JEV and PV is shown. Predictions (here onwards) are using the main model (M_4^1) unless explicitly specified. (*e*) $\Phi(\tau_F, \mu_R)$ evaluates the cellular infectivity at different values of compartment formation delay (τ_F) and degradation rate of viral (+)RNA in cytoplasm (μ_R) for PV at seeding, $N = 3$. (*f*) Fold change in Φ for PV infection corresponding to a change in various parameters with respect to the wild type (WT, table 1) values at different virus seeding (N) is shown. k_t^{WT}, k_c^{WT} and τ_F^{WT} correspond to estimates for PV (table 1), and μ_R^{WT}=0.25 h^{-1}.

(Φ), based on their life cycle parameters from our model (figure 4*d*). For example, we determine that Φ for JEV > PV > HCV and estimate the fraction of non-productive, single virus JEV and HCV infections are 40% and 85%, respectively. At larger viral seeding of $N = 8$, Φ for HCV is 0.95, closely matching the 95.3% infection success rate observed during an infection with 8 genomes per cell (as measured in the cell at 3 hpi [22]). Interestingly, while infection success rate with 10 seeding genomes remains unaffected when τ_F is increased by 2-fold, it drops by 50% for a single virus infection (figure 4*f*). This mirrors the larger reduction in fraction of productive PV infected cells observed due to action of membrane reorganization inhibitor PIK93 [67] at low multiplicity of infection [12]. This effect may also explain the enhanced activity observed when entry inhibitors (that would decrease effective virus seeding) are used in combination with other antiviral agents, like protease inhibitors, membrane reorganization inhibitors and cyclophilin inhibitors against HCV [68,69].

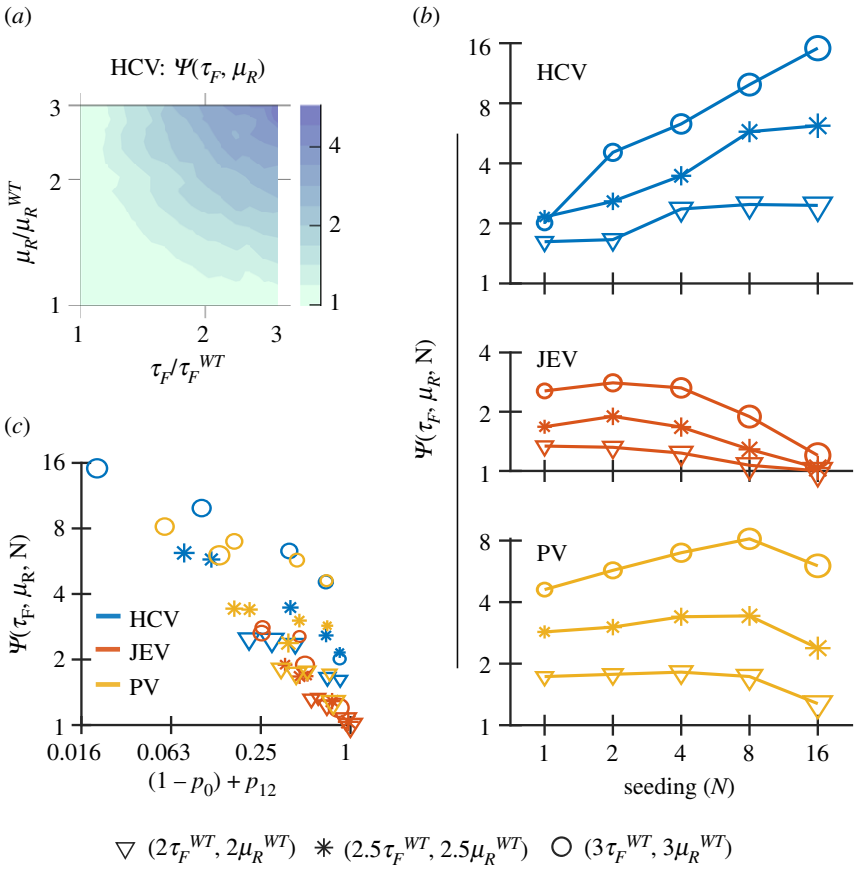

Figure 5. Synergy between life cycle processes affecting infectivity. (*a*) $\Psi(\tau_F, \mu_R)$ evaluates the Bliss synergy between τ_F and μ_R for Φ, for HCV at seeding $N = 3$. (*b*) Variation of $\Psi(\tau_F, \mu_R)$ for various fold change in parameter values (denoted by different markers) with viral seeding (N) for each virus is shown. (*c*) $\Psi(\tau_F, \mu_R)$ shows a negative correlation with $\{(1-p_0)+p_{12}\}$. τ_F^{WT} and τ_R^{WT} correspond to the estimate for the respective virus. Marker properties are same in (*b*) and (*c*) and marker size corresponds to value of N.

2.7. Synergy among strategies reducing cellular infectivity

Since the life cycle parameters that limit Φ collaborate in complex ways, we conjectured that their interdependence would give rise to synergy in their effect. We use the Bliss independence criterion [70] to evaluate this synergy (Ψ) since these early life cycle events are likely to occur independently at the molecular level. Apart from reducing Φ independently, τ_F and μ_R positively synergize ($\Psi_{\tau_F,\mu_R} > 1$) when combined for the viruses (figure 5*a*; electronic supplementary material, figure S16a,b). For example, doubling of both τ_F and μ_R values resulted in an eightfold reduction in Φ compared to the product of their independent actions in the case of HCV. Positive synergism is also predicted using the Loewe additivity model [71] (CI < 1; electronic supplementary material, figure S17). In our formalism, synergy stems from enhanced delays in the formation of compartments leading to increased exposure of viral RNA to cytosolic degradation. By extension, other RNA viruses that employ compartmentalization to stabilize replication should also display such behaviour.

At first glance, the quantitative relationship for $\tau_F - \mu_R$ synergy varies with the virus–host system and seeding density, in addition to the level of inhibition in a complicated fashion (figure 5*b*). However, we find that when $\Phi \to 1$ or is close to extinction of infection ($\Phi \to 0$), perturbations do not influence Φ, individually or in combination. More importantly, figure 5*c* shows that Ψ_{τ_F,μ_R} decreases with $\{(1 - p_0) + p_{12}\}$, a surrogate for how far the system is from either of the two deterministic limits (electronic supplementary material, S4), where p_0 and p_{12} denote Φ in unperturbed and doubly perturbed conditions, respectively. Similar synergy and associated negative correlation with $\{(1 - p_0) + p_{12}\}$ is also predicted for $\tau_F - k_t$ (electronic supplementary material, figure S16c-g). Therefore, interventions that target membrane reorganization can be combined with other antiviral inhibitors to target early life cycle events to achieve efficient viral clearance.

3. Discussion

We incorporated the dynamics of CM formation accompanying cellular infection into a simplified intracellular life cycle description for monopartite (+)RNA viruses. This allowed us to capture observed dynamics for viruses spanning multiple (+)RNA virus families, decipher the diverse effects of antivirals, host cell susceptibility, host factor silencing, virus mutations, as well as identify stochasticity associated with establishment of (+)RNA virus infection upon cell entry.

Based on temporal dependencies among model parameters, the viral life cycle can be categorized into three phases—establishment, growth and saturation (pseudo-steady state). High translation efficiency and fast CM formation, as observed for JEV, result in a short establishment phase. Following the compartmentalization of replication, the life cycle enters the growth phase that is marked by positive

feedback from the newly synthesized RNA fuelling the replication process. Kinetics of replication (k_r), (+)RNA export from CM (k_e) and (+)RNA degradation in cytoplasm shape this phase, which is short-lived for PV, owing to its high replication and export rates. We attribute the significantly large virus generation and release rate (k_a) for PV compared to the *Flaviviridae* members to differences in virus structural complexity, assembly and egress mechanisms [72,73]. Replicative fitness (partly defined by k_r and N_C) and viral RNA stability (μ_R^{-1}) determine the steady state levels of cytoplasmic (+)RNA and viral titre in the final saturation phase for all viruses. Not surprisingly, k_r, which is targeted by nucleoside inhibitors, remains a promising pan-viral drug target. Additionally, temporal sensitivity profiles suggest that the replication kinetics for JEV is more sensitive to inhibition compared to translation while the reverse is true for PV. Virus production is robust against reduction in assembly rate (k_a) for all the three viruses. Combined with steady-state analysis, this suggests that genomes are packaged efficiently compared to their effective synthesis and degradation and hence targeting early viral life cycle events is likely to be a prudent approach.

In our formalism, we also identify dynamics of CM formation (broadly defined by τ_F and k_c) to be a key kinetic barrier in the early stage of the (+)RNA virus life cycle and it has been aptly described as the 'load and choke point' [17]. We demonstrate that the ability of viruses to successfully establish an infection in the host cell is stochastic and this 'cellular infectivity' (Φ) is determined at the onset of the infection. Such early stochastic extinction of viral infection has been similarly suggested due to biological noise [13,14,26]. Using our model-based characterization of the viral life cycle, we are able to estimate this effect for the viruses. For synchronous co-infection, we predict that multiple genome infections are more likely to result in productive infection than single copy infection (as observed for PV [74]).

In a cell population, Φ quantifies the fraction of cells successfully infected upon entry of infectious viral particle(s) and correlates with the multiplicity of infection (MOI). As with MOI (discussed in [73]), Φ also depends on seeding density (N) and virus–host determinants. Factors like viral genome stability in cytoplasm (μ_R^{-1}) and kinetics of viral processes antecedent to formation of RC_{CM} affect productive infection. Indeed, drop in viral titres measured for translation-defective PV strains has been attributed to reduction in infectivity rather than growth defects [75]. Infectivity is highly sensitive to τ_F (compared to k_t or k_c). This agrees with the reduction in Φ observed when membrane reorganization is hindered independently [6,11]. Similarly, we speculate that the infectivity of a virus in a host cell can define its permissiveness [17,76,77].

Some of the early-infection parameters can also control cellular infectivity effectively in combination, displaying higher order effects due to their mutual action on common viral entities or processes. Our predictions are consistent with enhancements in antiviral activity observed for membrane reorganizing inhibitor at lower MOI [12] as well as synergy observed between cell entry inhibitors and several classes of antiviral agents against HCV [68,69]. Thus, strategies or drugs inhibiting CM formation, slowing translation, increasing viral degradation and reducing viral seeding, are expected to synergize in reducing infectivity. Host and viral heterogeneity would further accentuate this all-or-none dimorphism due to this intrinsic interdependence [13,15].

Decrease in overall viral production due to lower infectivity can reduce viral seeding for the subsequent rounds of infection. Due to its dependency on viral seeding, such reduction in infectivity can manifest in a compounding effect that reduces the effective basic reproduction number R_0 and leads to viral clearance. Therefore, cellular antiviral strategies that target cellular infectivity can be used in conjunction with other interventions (including action of innate immune response) that reduce the virus load. Overall, our general theoretical framework serves as a starting point for analysis of novel viruses with limited molecular level characterization, to generate insights into life cycle properties and bottlenecks, design of experimental studies and evaluate antiviral strategies.

4. Methods

4.1. Experimental data

All experimental datasets used were curated from literature. Data for estimation of τ_S were retrieved from [37–40]. Cellular life cycle dynamics data for HCV, JEV and PV were obtained from [19,22,32], respectively. JFH1 (sgHCV strain) transfection dynamics and polyprotein dynamics of HCV NS4B mutants were obtained from [5,17], respectively. Effect of RTN silencing on viral dynamics was curated from [5,7]. Figure digitization and data extraction were done using WebPlotDigitizer [78].

4.2. Model fitting

Estimation of parameter values was done using iterative approximate Bayesian computation (iABC) algorithm. It iteratively improves upon the current (or the prior) distribution of parameter values, based on the convergence of the χ^2 statistics, to fit model to the observed data (described in electronic supplementary material, SM1). Briefly, we use Latin hyper-cube sampling [43] to efficiently sample current parameter distribution in the multi-dimensional parameter space. The deviation between the model prediction (based on sampled parameters) and observed data is computed as $\chi^2 = \sum((\text{Prediction} - \text{Data})^2/\text{Var}(\text{Data}))$ [19,79]. To increase robustness against sampling bias, we add uniform noise to the distribution while sampling at every iteration. A sub-set of the parameter combinations with lowest χ^2 values is picked to update the parameter distribution estimation. For parameter estimation, we start with a uniform distribution, over the range of interest, as our prior estimate. However, to test the validity of parameter estimation and check for robustness against initial guess, we use the posterior estimated for HCV (during its unbiased parameter estimation) to bias the prior estimate for fitting the model to JEV and PV life cycle. We observe that estimated distributions are not very sensitive to the prior used (electronic supplementary material, figures S6 and S5).

Practical identifiability is defined as the pairwise correlation in values of parameter combinations derived from the final iteration of estimation [19]. In case variance was missing, we assumed a 25% relative error in the reported data to calculate χ^2 values. Further details on the algorithm, implementation and diagnostic analysis are provided in the electronic supplementary material, Methods.

4.3. Temporal sensitivity analysis

We used extended Fourier amplitude sensitivity test (eFAST) [61,80] to estimate the corresponding temporal sensitivity profile. Sensitivity indices for RC_{CM}, V_T and R_{cyt}, corresponding to a change of up to 10% in parameter values, were evaluated every 1.5 min through the course of the infection to generate the temporal profile.

4.4. Infectivity calculation and the semi-stochastic framework

To estimate cellular infectivity (Φ), stochastic realizations of the life cycle were implemented using the Gillespie algorithm [81], and classified as (a) successful infection (I_S) if RC_{CM} is formed, (b) failed infection (I_F) if all viral (+)RNA degrade and (c) inconclusive if neither happen within a stipulated time. Since the fate of infection was decided in all stochastic realizations for HCV life cycle (slowest of the three viruses) by 12 h, this was used for the simulation run time. We consider only the 'conclusive' realizations and define Φ as $\#(I_S)/(\#(I_S)+\#(I_F))$. Dynamics of f_{CM} is incorporated by updating it at every event or at steps of $0.05\tau_F$ (whichever is shorter). This limits the error due to discretization of f_{CM} to 6.5%.

As the life cycle starts with a few molecules and reaches almost 10^5 copy number at saturation, we adopt a semi-stochastic framework to make the simulations computationally tractable. The initial part of the life cycle is simulated in the stochastic domain, but when system size crosses a threshold we shift to the deterministic (ODE based) framework. We define system size as minimum of the copy number of the different viral RNA species, namely R_{cyt}, RC_{CM} and R_{CM}. Here, we use RNA species to define the system size as protein levels are higher than RNA, and viruses are produced only in the late infection phase. Varying the threshold for transition to deterministic framework, the mean predicted HCV viral RNA dynamics is identical when using threshold of 50, 250 or 10^5 (equivalent to a fully stochastic simulation for HCV life cycle; electronic supplementary material, figure S15), implying that a choice of threshold of 50 is sufficiently accurate to predict the system dynamics in our semi-stochastic simulations. In our simulations, unless explicitly mentioned, we use a transition of threshold of 50, and consider 10^4 independent realizations during analysis.

4.5. Bliss synergy (Ψ) calculation

To calculate synergy (Ψ) between two parameters, a_1 and a_2, that reduce Φ, we estimate p_0, p_1, p_2 and p_{12} as Φ corresponding to no change, change in parameter a_1, parameter a_2, and in both parameters, respectively. Synergy among parameters is given by $\Psi = g_1 \cdot g_2/g_{12}$ where g_X denotes p_X/p_0 for $X \in 1, 2, 12$ (Bliss criterion [70]).

Data accessibility. Codes for iABC fitting can be downloaded from our Github repository: https://github.com/hcharsh/iABC_fit/tree/master/%2BRNA_viral_lifecycle_fit.

Authors' contributions. Data extraction: H.C. and V.A.R. Model development, software and formal analysis: H.C. Conceptualization, result interpretation and original draft preparation: H.C., V.A.R. and R.R.

Competing interests. The authors declare that no competing interests exist.

Funding. This work was supported by the Indian Institute of Science Bangalore (R.R.), Wellcome Trust—DBT India Alliance intermediate fellowship (R.R.), Council of Scientific and Industrial Research fellowship (V.A.R.) and the Prime Minister Research Fellowship (H.C.).

Acknowledgements. We thank Narendra Dixit, Mohit Jolly, Sunaina Banerjee and Suraj Jagtap for valuable feedback on the manuscript.

References

1. Miller S, Krijnse-Locker J. 2008 Modification of intracellular membrane structures for virus replication. *Nat. Rev. Microbiol.* **6**, 363–374. (doi:10.1038/nrmicro1890)
2. den Boon JA, Ahlquist P. 2010 Organelle-like membrane compartmentalization of positive-strand RNA virus replication factories. *Annu. Rev. Microbiol.* **64**, 241–256. (doi:10.1146/annurev.micro.112408.134012)
3. Paul D, Bartenschlager R. 2013 Architecture and biogenesis of plus-strand RNA virus replication factories. *World J. Virol.* **2**, 32–48. (doi:10.5501/wjv.v2.i2.32)
4. Romero-Brey I, Bartenschlager R. 2014 Membranous replication factories induced by plus-strand RNA viruses. *Viruses* **6**, 2826–2857. (doi:10.3390/v6072826)
5. Wu MJ, Ke PY, Hsu JT, Yeh CT, Horng JT. 2014 Reticulon 3 interacts with NS4B of the hepatitis C virus and negatively regulates viral replication by disrupting NS4B self-interaction. *Cell. Microbiol.* **16**, 1603–1618. (doi:10.1111/cmi.12318)
6. Tang WF *et al.* 2007 Reticulon 3 binds the 2C protein of enterovirus 71 and is required for viral replication. *J. Biol. Chem.* **282**, 5888–5898. (doi:10.1074/jbc.M611145200)
7. Aktepe TE, Liebscher S, Prier JE, Simmons CP, Mackenzie JM. 2017 The host protein reticulon 3.1A is utilized by flaviviruses to facilitate membrane remodelling. *Cell Rep.* **21**, 1639–1654. (doi:10.1016/j.celrep.2017.10.055)
8. Lundin A *et al.* 2014 Targeting membrane-bound viral RNA synthesis reveals potent inhibition of diverse coronaviruses including the Middle East respiratory syndrome virus. *PLoS Pathog.* **10**, e1004166. (doi:10.1371/journal.ppat.1004166)
9. García-Nicolás O *et al.* 2018 The small-compound inhibitor K22 displays broad antiviral activity against different members of the family flaviviridae and offers potential as a panviral inhibitor. *Antimicrob. Agents Chemother.* **62**, e01206-18.
10. Berger C *et al.* 2014 Daclatasvir-like inhibitors of NS5A block early biogenesis of hepatitis C virus-induced membranous replication factories, independent of RNA replication. *Gastroenterology* **147**, 1094–1105. (doi:10.1053/j.gastro.2014.07.019)
11. Berger KL, Kelly SM, Jordan TX, Tartell MA, Randall G. 2011 Hepatitis C virus stimulates the phosphatidylinositol 4-kinase III alpha-dependent phosphatidylinositol 4-phosphate production that is essential for its replication. *J. Virol.* **85**, 8870–8883. (doi:10.1128/JVI.00059-11)
12. Schulte MB, Andino R. 2014 Single-cell analysis uncovers extensive biological noise in poliovirus replication. *J. Virol.* **88**, 6205–6212. (doi:10.1128/JVI.03539-13)
13. Heldt FS, Kupke SY, Dorl S, Reichl U, Frensing T. 2015 Single-cell analysis and stochastic modelling unveil large cell-to-cell variability in influenza A virus infection. *Nat. Commun.* **6**, 8938. (doi:10.1038/ncomms9938)
14. Srivastava R, You L, Summers J, Yin J. 2002 Stochastic vs. deterministic modeling of intracellular viral kinetics. *J. Theor. Biol.* **218**, 309–321. (doi:10.1006/jtbi.2002.3078)
15. Snijder B, Sacher R, Rämö P, Damm EM, Liberali P, Pelkmans L. 2009 Population context determines cell-to-cell variability in endocytosis and virus infection. *Nature* **461**, 520–523. (doi:10.1038/nature08282)
16. Dahari H, Ribeiro RM, Rice CM, Perelson AS. 2007 Mathematical modeling of subgenomic hepatitis C virus replication in Huh-7 cells. *J. Virol.* **81**, 750–760. (doi:10.1128/JVI.01304-06)
17. Binder M *et al.* 2013 Replication vesicles are load- and choke-points in the hepatitis C virus lifecycle. *PLoS Pathog.* **9**, e1003561. (doi:10.1371/journal.ppat.1003561)
18. Regoes RR, Crotty S, Antia R, Tanaka MM. 2005 Optimal replication of poliovirus within cells. *Am. Nat.* **165**, 364–373. (doi:10.1086/428295)
19. Schulte MB, Draghi JA, Plotkin JB, Andino R. 2015 Experimentally guided models reveal replication principles that shape the mutation distribution of RNA viruses. *Elife* **4**, e03753. (doi:10.7554/eLife.03753)
20. McLean AK, Luciani F, Tanaka MM. 2010 Trade-offs in resource allocation in the intracellular life-cycle of hepatitis C virus. *J. Theor. Biol.* **267**, 565–572. (doi:10.1016/j.jtbi.2010.09.031)
21. Clausznitzer D, Harnisch J, Kaderali L. 2016 Multi-scale model for hepatitis C viral load kinetics under treatment with direct acting antivirals. *Virus Res.* **218**, 96–101. (doi:10.1016/j.virusres.2015.09.011)
22. Aunins TR, Marsh KA, Subramanya G, Uprichard SL, Perelson AS, Chatterjee A. 2018 Intracellular hepatitis C virus modeling predicts infection

dynamics and viral protein mechanisms. *J. Virol.* **92**, e02098-17. (doi:10.1128/JVI.02098-17)

23. Zitzmann C, Schmid B, Ruggieri A, Perelson AS, Binder M, Bartenschlager R, Kaderali L. 2020 A coupled mathematical model of the intracellular replication of dengue virus and the host cell immune response to infection. *Front Microbiol.* **11**, 725. (doi:10.3389/fmicb.2020.00725)
24. Teufel AI, Liu W, Draghi JA, Cameron CE, Wilke CO. 2020 Uncovering modeling features of viral replication dynamics from high-throughput single-cell virology experiments. *bioRxiv*. (doi:10.1101/2020.07.09.195925)
25. Yin J, Redovich J. 2018 Kinetic modeling of virus growth in cells. *Microbiol. Mol. Biol. Rev.* **82**, e00066-17. (doi:10.1128/MMBR.00066-17)
26. Miyashita S, Ishibashi K, Kishino H, Ishikawa M. 2015 Viruses roll the dice: the stochastic behavior of viral genome molecules accelerates viral adaptation at the cell and tissue levels. *PLoS Biol.* **13**, e1002094. (doi:10.1371/journal.pbio.1002094)
27. Zitzmann C, Kaderali L. 2018 Mathematical analysis of viral replication dynamics and antiviral treatment strategies: from basic models to age-based multi-scale modeling. *Front. Microbiol.* **9**, 1546. (doi:10.3389/fmicb.2018.01546)
28. Perelson AS, Herrmann E, Micol F, Zeuzem S. 2005 New kinetic models for the hepatitis C virus. *Hepatology* **42**, 749–754. (doi:10.1002/hep.20882)
29. Nguyen T, Guedj J. 2015 HCV kinetic models and their implications in drug development. *CPT Pharmacometrics Syst. Pharmacol.* **4**, 231–242. (doi:10.1002/psp4.28)
30. Zimmer A, Katzir I, Dekel E, Mayo AE, Alon U. 2016 Prediction of multidimensional drug dose responses based on measurements of drug pairs. *Proc. Natl Acad. Sci. USA* **113**, 10 442–10 447. (doi:10.1073/pnas.1606301113)
31. Padmanabhan P, Dixit NM. 2015 Modeling suggests a mechanism of synergy between hepatitis C virus entry inhibitors and drugs of other classes. *CPT Pharmacometrics Syst. Pharmacol.* **4**, 445–453. (doi:10.1002/psp4.12005)
32. Uchil PD, Satchidanandam V. 2003 Characterization of RNA synthesis, replication mechanism, and in vitro RNA-dependent RNA polymerase activity of Japanese encephalitis virus. *Virology* **307**, 358–371. (doi:10.1016/S0042-6822(02)00130-7)
33. Limpens RWAL, van der Schaar HM, Kumar D, Koster AJ, Snijder EJ, van Kuppeveld FJM, Bárcena M. 2011 The transformation of enterovirus replication structures: a three-dimensional study of single- and double-membrane compartments. *mBio* **2**, e00166-11. (doi:10.1128/mBio.00166-11)
34. van der Hoeven B, Oudshoorn D, Koster AJ, Snijder EJ, Kikkert M, Bárcena M. 2016 Biogenesis and architecture of arterivirus replication organelles. *Virus Res.* **220**, 70–90. (doi:10.1016/j.virusres.2016.04.001)
35. Paul D, Romero-Brey I, Gouttenoire J, Stoitsova S, Krijnse-Locker J, Moradpour D, Bartenschlager R. 2011 NS4B self-interaction through conserved C-terminal elements is required for the establishment of functional hepatitis C virus replication complexes. *J. Virol.* **85**, 6963–6976. (doi:10.1128/JVI.00502-11)
36. Wagner TL, Wu H-I, Sharpe PJH, Coulson RN. 1984 Modeling distributions of insect development time: a literature review and application of the Weibull function. *Ann. Entomol. Soc. Am.* **77**, 475–483. (doi:10.1093/aesa/77.5.475)
37. Knoops K, Bárcena M, Limpens RWAL, Koster AJ, Mommaas AM, Snijder EJ. 2012 Ultrastructural characterization of arterivirus replication structures: reshaping the endoplasmic reticulum to accommodate viral RNA synthesis. *J. Virol.* **86**, 2474–2487. (doi:10.1128/JVI.06677-11)
38. Ulasli M, Verheije MH, de Haan CA, Reggiori F. 2010 Qualitative and quantitative ultrastructural analysis of the membrane rearrangements induced by coronavirus. *Cell. Microbiol.* **12**, 844–861. (doi:10.1111/j.1462-5822.2010.01437.x)
39. Romero-Brey I *et al.* 2012 Three-dimensional architecture and biogenesis of membrane structures associated with hepatitis C virus replication. *PLoS Pathog.* **8**, e1003056. (doi:10.1371/journal.ppat.1003056)
40. Cortese M *et al.* 2017 Ultrastructural characterization of Zika virus replication factories. *Cell Rep.* **18**, 2113–2123. (doi:10.1016/j.celrep.2017.02.014)
41. Münster M, Płaszczyca A, Cortese M, Neufeldt CJ, Goellner S, Long G, Bartenschlager R. 2018 A reverse genetics system for Zika virus based on a simple molecular cloning strategy. *Viruses* **10**, 368. (doi:10.3390/v10070368)
42. Brandenburg B, Lee LY, Lakadamyali M, Rust MJ, Zhuang X, Hogle JM. 2007 Imaging poliovirus entry in live cells. *PLoS Biol.* **5**, e183. (doi:10.1371/journal.pbio.0050183)
43. McKay MD, Beckman RJ, Conover WJ. 2000 A comparison of three methods for selecting values of input variables in the analysis of output from a computer code. *Technometrics* **42**, 55–61. (doi:10.1080/00401706.2000.10485979)
44. Oh JW, Ito T, Lai MM. 1999 A recombinant hepatitis C virus RNA-dependent RNA polymerase capable of copying the full-length viral RNA. *J. Virol.* **73**, 7694–7702. (doi:10.1128/JVI.73.9.7694-7702.1999)
45. Cleaves GR, Ryan TE, Schlesinger RW. 1981 Identification and characterization of type 2 dengue virus replicative intermediate and replicative form RNAs. *Virology* **111**, 73–83. (doi:10.1016/0042-6822(81)90654-1)
46. Wang H, Tai AW. 2017 Continuous de novo generation of spatially segregated hepatitis C virus replication organelles revealed by pulse-chase imaging. *J. Hepatol.* **66**, 55–66. (doi:10.1016/j.jhep.2016.08.018)
47. Grünvogel O *et al.* 2018 Secretion of hepatitis C virus replication intermediates reduces activation of Toll-Like receptor 3 in hepatocytes. *Gastroenterology* **154**, 2237–2251. (doi:10.1053/j.gastro.2018.03.020)
48. Wang C, Pflugheber J, Sumpter R, Sodora DL, Hui D, Sen GC, Gale M. 2003 Alpha interferon induces distinct translational control programs to suppress hepatitis C virus RNA replication. *J. Virol.* **77**, 3898–3912. (doi:10.1128/JVI.77.7.3898-3912.2003)
49. Robinson M, Yang H, Sun S-C, Peng B, Tian Y, Pagratis N, Greenstein AE, Delaney WE. 2010 Novel hepatitis C virus reporter replicon cell lines enable efficient antiviral screening against genotype 1A. *Antimicrob. Agents Chemother.* **54**, 3099–3106. (doi:10.1128/AAC.00289-10)
50. Arnold JJ, Cameron CE. 2000 Poliovirus RNA-dependent RNA polymerase (3D(pol)). Assembly of stable, elongation-competent complexes by using a symmetrical primer-template substrate (sym/sub). *J. Biol. Chem.* **275**, 5329–5336. (doi:10.1074/jbc.275.8.5329)
51. Baltimore D. 1968 Structure of the poliovirus replicative intermediate RNA. *J. Mol. Biol.* **32**, 359–368. (doi:10.1016/0022-2836(68)90015-6)
52. Richards OC, Martin SC, Jense HG, Ehrenfeld E. 1984 Structure of poliovirus replicative intermediate RNA. Electron microscope analysis of RNA cross-linked in vivo with psoralen derivative. *J. Mol. Biol.* **173**, 325–340. (doi:10.1016/0022-2836(84)90124-4)
53. Liu L, Dong H, Chen H, Zhang J, Ling H, Li Z, Shi PY, Li H. 2010 Flavivirus RNA cap methyltransferase: structure, function, and inhibition. *Front. Biol. (Beijing)* **5**, 286–303. (doi:10.1007/s11515-010-0660-y)
54. Pelletier J, Sonenberg N. 1988 Internal initiation of translation of eukaryotic mRNA directed by a sequence derived from poliovirus RNA. *Nature* **334**, 320–325. (doi:10.1038/334320a0)
55. Tsukiyama-Kohara K, Iizuka N, Kohara M, Nomoto A. 1992 Internal ribosome entry site within hepatitis C virus RNA. *J. Virol.* **66**, 1476–1483. (doi:10.1128/jvi.66.3.1476-1483.1992)
56. Kuhn RJ *et al.* 2002 Structure of dengue virus: implications for flavivirus organization, maturation, and fusion. *Cell* **108**, 717–725. (doi:10.1016/S0092-8674(02)00660-8)
57. Schüttler CG, Thomas C, Discher T, Friese G, Lohmeyer J, Schuster R, Schaefer S, Gerlich WH. 2004 Variable ratio of hepatitis C virus RNA to viral core antigen in patient sera. *J. Clin. Microbiol.* **42**, 1977–1981. (doi:10.1128/JCM.42.5.1977-1981.2004)
58. Lin JY, Chen TC, Weng KF, Chang SC, Chen LL, Shih SR. 2009 Viral and host proteins involved in picornavirus life cycle. *J. Biomed. Sci.* **16**, 103. (doi:10.1186/1423-0127-16-103)
59. Keum SJ, Park SM, Park JH, Jung JH, Shin EJ, Jang SK. 2012 The specific infectivity of hepatitis C virus changes through its life cycle. *Virology* **433**, 462–470. (doi:10.1016/j.virol.2012.08.046)
60. Ivanisenko NV *et al.* 2014 A new stochastic model for subgenomic hepatitis C virus replication considers drug resistant mutants. *PLoS ONE* **9**, e91502. (doi:10.1371/journal.pone.0091502)
61. Marino S, Hogue IB, Ray CJ, Kirschner DE. 2008 A methodology for performing global uncertainty and sensitivity analysis in systems biology. *J. Theor. Biol.* **254**, 178–196. (doi:10.1016/j.jtbi.2008.04.011)
62. Gouttenoire J, Roingeard P, Penin F, Moradpour D. 2010 Amphipathic α-helix AH2 is a major determinant for the oligomerization of hepatitis C virus nonstructural protein 4B. *J. Virol.* **84**, 12 529–12 537. (doi:10.1128/JVI.01798-10)

63. Diaz A, Wang X, Ahlquist P. 2010 Membrane-shaping host reticulon proteins play crucial roles in viral RNA replication compartment formation and function. *Proc. Natl Acad. Sci. USA* **107**, 16 291–16 296. (doi:10.1073/pnas.1011105107)
64. Diaz A, Ahlquist P. 2012 Role of host reticulon proteins in rearranging membranes for positive-strand RNA virus replication. *Curr. Opin. Microbiol.* **15**, 519–524. (doi:10.1016/j.mib.2012.04.007)
65. Berger KL, Cooper JD, Heaton NS, Yoon R, Oakland TE, Jordan TX, Mateu G, Grakoui A, Randall G. 2009 Roles for endocytic trafficking and phosphatidylinositol 4-kinase III alpha in hepatitis C virus replication. *Proc. Natl Acad. Sci. USA* **106**, 7577–7582. (doi:10.1073/pnas.0902693106)
66. Berger KL, Randall G. 2009 Potential roles for cellular cofactors in hepatitis C virus replication complex formation. *Commun. Integr. Biol.* **2**, 471–473. (doi:10.4161/cib.2.6.9261)
67. Arita M, Kojima H, Nagano T, Okabe T, Wakita T, Shimizu H. 2011 Phosphatidylinositol 4-kinase III beta is a target of enviroxime-like compounds for antipoliovirus activity. *J. Virol.* **85**, 2364–2372. (doi:10.1128/JVI.02249-10)
68. Zhu H, Wong-Staal F, Lee H, Syder A, McKelvy J, Schooley RT, Wyles DL. 2012 Evaluation of ITX 5061, a scavenger receptor B1 antagonist: resistance selection and activity in combination with other hepatitis C virus antivirals. *J. Infect. Dis.* **205**, 656–662. (doi:10.1093/infdis/jir802)
69. Xiao F *et al.* 2015 Synergy of entry inhibitors with direct-acting antivirals uncovers novel combinations for prevention and treatment of hepatitis C. *Gut* **64**, 483–494. (doi:10.1136/gutjnl-2013-306155)
70. Bliss CI. 1939 The toxicity of poisons applied jointly 1. *Ann. Appl. Biol.* **26**, 585–615. (doi:10.1111/j.1744-7348.1939.tb06990.x)
71. Loewe S. 1953 The problem of synergism and antagonism of combined drugs. *Arzneimittelforschung* **3**, 285–290.
72. Comas-Garcia M. 2019 Packaging of genomic RNA in positive-sense single-stranded RNA viruses: a complex story. *Viruses* **11**, 253. (doi:10.3390/v11030253)
73. Song Y *et al.* 2017 Limits of variation, specific infectivity, and genome packaging of massively recoded poliovirus genomes. *Proc. Natl Acad. Sci. USA* **114**, E8731–E8740. (doi:10.1073/pnas.1714385114)
74. Aguilera ER, Erickson AK, Jesudhasan PR, Robinson CM, Pfeiffer JK. 2017 Plaques formed by mutagenized viral populations have elevated coinfection frequencies. *mBio* **8**, e02020-16. (doi:10.1128/mBio.02020-16)
75. Coleman JR, Papamichail D, Skiena S, Futcher B, Wimmer E, Mueller S. 2008 Virus attenuation by genome-scale changes in codon pair bias. *Science* **320**, 1784–1787. (doi:10.1126/science.1155761)
76. Lohmann V, Hoffmann S, Herian U, Penin F, Bartenschlager R. 2003 Viral and cellular determinants of hepatitis C virus RNA replication in cell culture. *J. Virol.* **77**, 3007–3019. (doi:10.1128/JVI.77.5.3007-3019.2003)
77. Blight KJ, McKeating JA, Rice CM. 2002 Highly permissive cell lines for subgenomic and genomic hepatitis C virus RNA replication. *J. Virol.* **76**, 13 001–13 014. (doi:10.1128/JVI.76.24.13001-13014.2002)
78. Rohatgi A. 2020 Webplotdigitizer: Version 4.3.
79. Beaumont MA, Zhang W, Balding DJ. 2002 Approximate Bayesian computation in population genetics. *Genetics* **162**, 2025–2035. (doi:10.1093/genetics/162.4.2025)
80. Saltelli A, Bolado R. 1998 An alternative way to compute Fourier amplitude sensitivity test (FAST). *Comput. Stat. Data Anal.* **26**, 445–460. (doi:10.1016/S0167-9473(97)00043-1)
81. Gillespie DT. 1977 Exact stochastic simulation of coupled chemical reactions. *J. Phys. Chem.* **81**, 2340–2361. (doi:10.1021/j100540a008)